Electronic spin transitions and the seismic properties of ferrous iron-bearing MgSiO$_3$ post-perovskite

Stephen Stackhouse,[1] John P. Brodholt,[1] David P. Dobson,[1] and G. David Price[1]

[1] The elastic constants of post-perovskite of chemical composition Mg$_{0.9375}$Fe$_{0.0625}$SiO$_3$ and Mg$_{0.8750}$Fe$_{0.1250}$SiO$_3$ have been calculated at 0 K and 136 GPa using ab initio methods. For both compositions studied, iron remains in a high-spin state below 180 GPa at 0 K. The effect of spin state on elastic properties is small. Logarithmic derivations of isotropic wave velocities and density with respect to ferrous iron content are similar to those predicted from pure end-members. **Citation:** Stackhouse, S., J. P. Brodholt, D. P. Dobson, and G. D. Price (2006), Electronic spin transitions and the seismic properties of ferrous iron-bearing MgSiO$_3$ post-perovskite, *Geophys. Res. Lett.*, *33*, L12S03, doi:10.1029/2005GL025589.

1. Introduction

[2] The bulk of the lower mantle is believed to be composed of iron-bearing magnesium silicate perovskite [*Liu*, 1975; *Knittle and Jeanloz*, 1997], coexisting with small amounts of magnesiowüstite and calcium silicate perovskite [*Lee et al.*, 2004], which transforms to a post-perovskite phase 200–400 km from the bottom [*Murakami et al.*, 2005; *Ono and Oganov*, 2005]. Deeper still, 5–20 km thick ultra-low velocity zones at the base of the mantle [*Garnero and Helmberger*, 1995] are postulated to comprise iron enriched post-perovskite [*Mao et al.*, 2005], iron-rich partial melt [*Rost et al.*, 2005], or relics of banded iron formation [*Dobson and Brodholt*, 2005]. In view of the ubiquitous nature of iron in the lower mantle, it is important to know how it may affect the properties of mantle phases, in order to accurately interpret seismic observations and construct good geophysical models.

[3] To estimate the effect of iron on the properties of minerals in the lower mantle is quite complex. Not only does one need to know the amount of iron present in the various phases, but also its crystallographic site, oxidation-state and spin-state. The latter has become of increasing interest since it was shown that iron in both magnesiowüstite and perovskite undergoes a high to low-spin transition under lower mantle pressures [*Badro et al.*, 2003, 2004]. The implications of these transitions may be significant. Because the spin state of iron affects its ionic radius, it could influence partitioning, which could, in turn, lead to seismic discontinuities [*Badro et al.*, 2003]. The spin state of iron in magnesiowüstite also has a large effect on its elastic properties [*Lin et al.*, 2005], which again could affect lower mantle velocity structure. In addition, it is postulated that

because lower mantle minerals incorporating iron in a low-spin state have a higher radiative thermal conductivity than those incorporating iron in a high-spin state, a high to low-spin transition will increase radiative thermal conductivity, hinder convection and favor mantle layering [*Badro et al.*, 2004].

[4] Investigations of the elastic properties of pure end-member FeSiO$_3$ post-perovskite found iron to be in a high-spin anti-ferromagnetic state at mantle pressures [*Caracas and Cohen*, 2005; *Stackhouse et al.*, 2006], but the spin state for lower and more appropriate concentrations is not known. In addition, because pure end-member FeSiO$_3$ post-perovskite was found to be dynamically unstable with iron in a low-spin state, its elastic properties could not be determined. Therefore at present we have no estimate of the extent to which the elastic properties of iron-bearing post-perovskite phase changes as iron goes from a high to low-spin state.

[5] Here we report the results of *ab initio* calculations on post-perovskite with composition Mg$_{0.9375}$Fe$_{0.0625}$SiO$_3$, similar to that expected in the lowermost mantle [*Murakami et al.*, 2005], and Mg$_{0.8750}$Fe$_{0.1250}$SiO$_3$. Estimated spin transition pressures for iron are presented for both post-perovskite compositions, along with the elastic properties with iron in both spin states. The possible geophysical implications of these are discussed, in particular, with regard to seismic discontinuities and mantle dynamics.

2. Computational Details

[6] It is well known that standard density functional methods fail to predict the correct band structure of strongly correlated systems (typically those containing metal ions with partially filled d or f shells). For example, both Fe$_2$SiO$_4$ [*Coccoccioni et al.*, 2003] and FeO [*Alfredsson et al.*, 2004] are predicted to be metals when they are insulators. This has led to the use of advanced techniques, such as hybrid functionals [*Alfredsson et al.*, 2004], which compute their correct band structure. It is often assumed, however, that although standard density functional methods are unable to determine accurate band structure, they may still be employed to calculate other important properties such as magnetic state, lattice parameters, bulk and shear moduli. Several studies using density functional methods to determine the spin state of iron in pertinent minerals [*Cococcioni et al.*, 2003; *Li et al.*, 2005a] have found good agreement with experiment. Others have used them to calculate the elastic properties of iron-bearing silicate perovskite [*Li et al.*, 2005b]. Further calculations using mixed functionals are necessary to confirm the validity of our results.

[7] Experimental studies of iron partitioning amongst lower mantle mineral phases [*Murakami et al.*, 2005;

---

[1]Department of Earth Sciences, University College London, London, UK.

Table 1. Initial Fractional Coordinates and Separation of Ferrous Iron in $Mg_{0.8750}Fe_{0.1250}SiO_3$ Post-Perovskite Models

Model	Fe_{Mg} ($Mg^{2+} \rightarrow Fe^{2+}$)	$Fe_{Mg'}$ ($Mg^{2+} \rightarrow Fe^{2+}$)	$d(Fe_{Mg} - Fe_{Mg'})$/Å
SSM1	(0.25, 0.75, 0.75)	(0.50, 0.75, 0.75)	2.461
SSM2	(0.00, 0.25, 0.25)	(0.50, 0.75, 0.75)	7.020
SSM3	(0.25, 0.75, 0.75)	(0.75, 0.75, 0.75)	4.922
SSM4	(0.25. 0.75, 0.75)	(0.38, 0.75, 0.25)	3.286
SSM5	(0.25, 0.75, 0.75)	(0.13, 0.25, 0.75)	4.203

Kobayashi et al., 2005] suggest that at the core-mantle boundary post-perovskite will have an Fe/(Mg + Fe) ratio of only a few percent. No data is available on the partitioning of iron between the different crystallographic sites, its oxidation-state or spin-state. In view of this, we decided, in the first instance, to investigate post-perovskite with ferrous iron located in the magnesium sites. This is a reasonable first step, since in perovskite it is estimated that fifty percent of iron is of this type [*McCammon*, 1997]. Therefore an eighty atom, $4 \times 1 \times 1$ supercell, of magnesium silicate post-perovskite, incorporating one iron for magnesium substitution, was constructed. In addition to this, five other models of identical size that contained two iron substitutions were also made. The exact substitution sites and names to which the models will subsequently be referred are listed in Table 1. For an eighty atom cell one and two iron for magnesium substitutions represent Fe/(Mg + Fe) ratios of 6.25 and 12.5 percent. Together with previous results for the pure end-members, this allows us to interpolate over all reasonable iron concentrations.

[8] Simulations were performed using the projector-augmented-wave implementation [*Blöchl*, 1994; *Kresse and Joubert*, 1999] of the density functional theory based VASP code [*Kresse and Furthmüller*, 1996]. The exchange-correlation functional used adhered to the PW91 form of the generalized gradient approximation [*Wang and Perdew*, 1991; *Perdew et al.*, 1992]. To determine spin transition pressures, each of the models was optimized with ferrous iron in selected spin states, over the pressure range 80–160 GPa, using a plane-wave cut-off of 1500 eV and a $2 \times 2 \times 2$ Monkhorst-Pack grid [*Monkhorst and Pack*, 1976]. This ensured that enthalpy differences were converged to 0.1 meV per atom. To determine athermal elastic constants three different orthorhombic and one triclinic strain, of magnitude ±0.3, ±0.7 and ±1.0 percent were applied to optimized models, the induced stresses calculated and stress-strain relation fit to a second-order polynomial. For elastic constants calculations the plane-wave cut-off was reduced to 1000 eV and Brillouin zone sampling

restricted to the Γ- point. Employing a larger plane-wave cut-off of 1500 eV and $2 \times 2 \times 2$ Monkhorst-Pack grid caused calculated elastic constants to differ by an average of about one percent and the bulk and shear modulus by less than a quarter of a percent.

3. Results and Discussion

[9] The calculated enthalpies of the five post-perovskite models incorporating two ferrous iron substitutions are listed in Table 2. One can see that, at a given pressure, there is a small difference of about 0.5 meV per atom in the enthalpies of the five different substitution configurations. This is less than that for different arrangements of ferric iron charge coupled with aluminum in perovskite [*Li et al.*, 2005a], probably because substitution of ferrous iron does not result in an unfavorable charge separation. Therefore each of the substitution configurations has an equal chance of occurring.

[10] It is interesting to note that although each of the substitution configurations is of similar probability, they exhibit a wide range of transition pressures, listed in Table 3. These can be explained in terms of proximity of the cations and tilting of silica octahedra during compression. In the post-perovskite structure the metal cations lie between sheets of linked silica octahedra. The predominant mechanism by which spin transitions are expected to be induced is, therefore, from the silica sheets pushing on the iron cations during compression. It is also important to note that the octahedra are edge-sharing along the *a* direction and corner-sharing along the *c* direction. This means that compression along the *a* direction causes the octahedra to tilt within the plane, while that in the *c* direction causes them to tilt in such a way that they push bridging oxygen atoms into the interlayer space, confining the metal cations. The spin transition pressures of the SSM2, SSM3 and SSM5 configurations are similar to that of the model with a single iron substitution, because the substitutions sites are far apart and effectively isolated. The SSM1 configuration, however, has a very high spin transition pressure due to the fact that the cations lie close to each other along the *a* direction, holding the silicate layers apart much more effectively than an individual cation. In the SSM4 configuration, the two cations lie adjacent to one another, along the *c* direction, but although this hinders closing of the

Table 2. Calculated Preferred Spin State and Enthalpy for Each $Mg_{0.8750}Fe_{0.1250}SiO_3$ Model at Selected Pressures

Model	Spin State		H/eV	
	Fe_{Mg}	$Fe_{Mg'}$	80 GPa	160 GPa
SSM1	4/2	4/2	−269.03	−20.02
SSM2	4/2	4/2	−269.06	−20.04
SSM3	4/2	4/2	−269.08	−20.02
SSM4	4/2	4/2	−269.06	−20.05
SSM5	4/2	4/2	−269.05	−20.01

Table 3. Calculated Spin Transitions and Their Corresponding Pressures for Ferrous Iron in Post-Perovskite

Model	Spin Transition					P_T/GPa
	Fe_{Mg}	Fe_{Mgi}	$\rightarrow$	Fe_{Mg}	$Fe_{Mg'}$	
		$Mg_{0.9375}Fe_{0.0625}SiO_3$				
	4/2	-	$\rightarrow$	0/2	-	230
		$Mg_{0.8750}Fe_{0.1250}SiO_3$				
SSM1	4/2	4/2	$\rightarrow$	0/2	0/2	288
SSM2	4/2	4/2	$\rightarrow$	0/2	0/2	233
SSM3	4/2	4/2	$\rightarrow$	0/2	0/2	239
SSM4	4/2	4/2	$\rightarrow$	0/2	0/2	183
SSM5	4/2	4/2	$\rightarrow$	0/2	0/2	211
		$FeSiO_3$[a]				
	4/2	−4/2	$\rightarrow$	0/2	0/2	356

[a]Determined using data from *Stackhouse et al.* [2006].

Table 4. Calculated Density and 0 K Elastic Moduli of Iron-Bearing MgSiO$_3$ Post-Perovskite (in GPa)

P/GPa	Spin State		ρ/g cm^{-3}	C_{11}	C_{22}	C_{33}	C_{12}	C_{13}	C_{23}	C_{44}	C_{55}	C_{66}	K	G
	Fe$_{Mg}$	Fe$_{Mg'}$												
						MgSiO$_3$[a]								
136	-	-	5.528	1332	995	1318	461	362	525	291	279	442	702	345
						Mg$_{0.9375}$Fe$_{0.0625}$SiO$_3$								
136	0/2	-	5.631	1331	992	1314	477	360	526	297	270	451	705	344
136	4/2	-	5.624	1326	992	1320	474	362	525	293	275	437	704	343
					Mg$_{0.8750}$Fe$_{0.1250}$SiO$_3$ − SSM2 Model									
136	0/2	−0/2	5.729	1318	987	1302	488	369	528	290	237	426	706	327
136	4/2	−4/2	5.716	1311	989	1317	482	372	525	288	271	431	706	337
136	4/2	−4/2	5.716	1311	989	1317	482	372	525	288	271	431	706	337
					Mg$_{0.8750}$Fe$_{0.1250}$SiO$_3$ − SSM4 Model									
136	0/2	−0/2	5.732	1319	983	1304	489	369	528	285	247	433	706	329
136	4/2	−4/2	5.718	1310	987	1318	483	372	524	289	272	429	706	337
136	4/2	−4/2	5.716	1311	989	1316	483	372	525	288	271	431	706	337
						FeSiO$_3$[b]								
136	4/2	−4/2	6.947	1174	993	1236	543	486	550	192	221	320	727	261

[a]Taken from *Stackhouse et al.* [2005].
[b]Taken from *Stackhouse et al.* [2006].

layers, as the layers are compressed the tilting of the silica octahedra pushes them into one another, thereby lowering their spin transition pressure.

[11] Our results indicate that, in post-perovskite, ferrous iron remains in a high-spin state up to 180 GPa at 0 K. Taking into account temperature is expected to increase transition pressures [*Badro et al.*, 2004]. According to the arguments of *Badro et al.* [2004], this could mean that radiative thermal conductivity will be low in the lower mantle. This should be taken into account when considering the dynamics of the lower mantle. The spin state of ferric iron in post-perovskite, under lower mantle conditions, is unknown. Further work must be done to investigate this.

[12] Elastic constants for selected post-perovskite models are reported in Table 4. Incorporation of iron into MgSiO$_3$ post-perovskite results in an expected density increase, a larger bulk modulus and lower shear modulus. This confirms previous work [*Stackhouse et al.*, 2006] where the affect of incorporating ferrous iron on the elastic and seismic properties of MgSiO$_3$ post-perovskite was estimated from linear mixing of end-member properties. Figure 1

shows how compressional (V_P), shear (V_S) and bulk (V_Φ) isotropic wave velocities of post-perovskite vary as a function of ferrous iron content. Solid lines represent values calculated from linear mixing of densities, bulk and shear moduli of the MgSiO$_3$ and FeSiO$_3$ end-members, taken from *Stackhouse et al.* [2005, 2006], while markers show values from the present study. One can see that, linear mixing provides excellent estimates of seismic velocities. This validates previous estimations of the seismic properties of an iron-rich post-perovskite phase [*Stackhouse et al.*, 2006], which were found to be compatible with those often seen for ultra-low velocity zones. Useful derivatives of elastic and seismic properties of post-perovskite with respect to ferrous iron content are given in Table 5. The slight affect of small amounts of iron on the seismic properties of post-perovskite strengthens previous arguments for the compatibility of the phase with observations for the lower-most mantle [*Wookey et al.*, 2005].

[13] The spin state of iron appears to have only a small effect on the elastic properties of post-perovskite, at least when present in the small fractions studied here. This is similar to observations for ferric iron in perovskite [*Li et al.*, 2005b]. It is surprising in light of recent experimental work reporting it to have a large effect on the bulk modulus of magnesiowüstite (composition Mg$_{0.83}$Fe$_{0.17}$O) [*Lin et al.*,

Figure 1. Decrease in compressional (V_P), shear (V_S) and bulk (V_Φ) isotropic wave velocities for post-perovskite as a function of ferrous iron content at 136 GPa and 0 K. Solid lines represent values calculated from linear mixing of pure end-member properties, taken from *Stackhouse et al.* [2005, 2006], while markers show values calculated for models incorporating an explicit percentage of iron.

Table 5. Derivatives of Seismic Properties and Density of (Mg, Fe)SiO$_3$ Post-Perovskite With Respect to Iron Content at 136 GPa and 0 K[a]

	Derivative
$\partial \ln \rho / \partial Fe$	0.2261
$\partial \ln K / \partial Fe$	0.0349
$\partial \ln G / \partial Fe$	−0.2870
$\partial \ln V_P / \partial Fe$	−0.1532
$\partial \ln V_S / \partial Fe$	−0.2566
$\partial \ln V_\Phi / \partial Fe$	−0.0956

[a]Fe = fraction of Mg substituted by Fe.
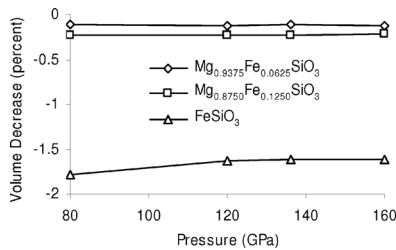
Figure 2. Difference in volume for post-perovskite containing ferrous iron in a high and low-spin state at 0 K, as a function of composition and pressure. FeSiO₃ values taken from *Stackhouse et al.* [2006].

2005]. It is important to note, however, that for a given iron to magnesium ratio, the volume fraction of iron in magnesiowüstite is two and a half times that of post-perovskite, due to their different formula units. In addition, the authors of the experimental investigation [*Lin et al.*, 2005] report the contrast between the bulk moduli at 60 GPa. One can see in Figure 2 how the volume difference for post-perovskite containing ferrous iron in a high and a low-spin state increases with iron content, but decreases with pressure. One should, therefore, perhaps not expect such a large contrast in bulk modulus in post-perovskite at 136 GPa, as that reported for magnesiowüstite at 60 GPa [*Lin et al.*, 2005].

[14]   In conclusion, ferrous iron incorporated into magnesium silicate post-perovskite is expected to be in a high-spin state across the entire pressure range of the lower mantle, and this should be taken into account when considering the dynamics of the region. Incorporation of low amounts of ferrous iron into the post-perovskite phase has only a slight affect on its elastic properties, irrespective of spin state, which are compatible with seismic observations for the lowermost mantle.

References

Alfredsson, M., G. D. Price, C. R. A. Catlow, S. C. Parker, R. Orlando, and J. P. Brodholt (2004), Electronic structure of the antiferromagnetic *B1*–structured FeO, *Phys. Rev. B.*, *70*, 165111.

Badro, J., G. Fiquet, F. Guyot, J.-P. Rueff, V. V. Struzhkin, G. Vankó, and G. Monaco (2003), Iron partitioning in Earth's mantle: Toward a Deep lower mantle discontinuity, *Science*, *300*, 789–791.

Badro, J., J.-P. Rueff, G. Vankó, G. Monaco, G. Fiquet, and F. Guyot (2004), Electronic transitions in perovskite: Possible nonconvecting layers in the lower mantle, *Science*, *305*, 383–386.

Blöchl, P. R. (1994), Projector augmented-wave method, *Phys. Rev. B.*, *50*, 17,953–17,979.

Caracas, R., and R. E. Cohen (2005), Effect of chemistry on the stability and elasticity of the perovskite and post-perovskite phases in the MgSiO₃-FeSiO₃-Al₂O₃ system and implications for the lowermost mantle, *Geophys. Res. Lett.*, *32*, L16310, doi:10.1029/2005GL023164.

Cococcioni, M., S. Dal Corso, and S. de Gironcoli (2003), Structural, electronic and magnetic properties of Fe₂SiO₄ fayalite: Comparison of LDA and GGA results, *Phys. Rev. B*, *67*, 094106.

Dobson, D., and J. P. Brodholt (2005), Subducted banded iron formations as a source of ultralow-velocity zones at the core-mantle boundary, *Nature*, *434*, 371–374.

Garnero, E. J., and D. V. Helmberger (1995), A very low basal layer underlying large-scale low-velocity anomalies in the lower mantle beneath the Pacific: Evidence from core phases, *Phys. Earth Planet Int.*, *91*, 161–176.

Knittle, E., and R. Jeanloz (1997), Synthesis and equation of state of (Mg, Fe)SiO₃ perovskite to over 100 gigapascals, *Science*, *235*, 668–670.

Kobayashi, Y., T. Kondo, E. Ohtani, N. Hirao, N. Miyajima, T. Yagi, T. Nagase, and T. Kikegawa (2005), Fe-Mg partitioning between (Mg, Fe)SiO₃ post-perovskite, perovskite, and magnesiowüstite in the Earth's lower mantle, *Geophys. Res. Lett.*, *32*, L19301, doi:10.1029/2005GL023257.

Kresse, G., and J. Furthmüller (1996), Efficient interative schemes for ab initio total-energy calculations using a plane-wave basis set, *Phys. Rev. B*, *54*, 11,169–11,186.

Kresse, G., and D. Joubert (1999), From ultrasoft pseudopotentials to the projector augmented-wave method, *Phys. Rev. B*, *59*, 1758–1775.

Lee, K. K. M., B. O'Neill, W. R. Panero, S.-H. Shim, L. R. Benedetti, and R. Jeanloz (2004), Equation of state of the high-pressure phases of a natural peridotite and implications for the Earth's lower mantle, *Earth Planet. Sci. Lett.*, *223*, 381–393.

Li, L., J. P. Brodholt, S. Stackhouse, D. J. Weidner, M. Alfredsson, and G. D. Price (2005a), Electronic spin state of ferric iron in Al-bearing perovskite in the lower mantle, *Geophys. Res. Lett.*, *32*, L17307, doi:10.1029/2005GL023045.

Li, L., J. P. Brodholt, S. Stackhouse, D. Weidner, M. Alfredsson, and G. D. Price (2005b), Elasticity of (Mg, Fe) (Si, Al)O₃-perovskite at high pressure, *Earth Planet. Sci. Lett.*, *240*, 529–536.

Lin, J.-F., V. V. Struzhkin, S. D. Jacobson, M. Y. Hu, P. Chow, J. Kung, H. Liu, H.-K. Mao, and R. J. Hemley (2005), Spin transition of iron in magnesiowüstite in the Earth's lower mantle, *Nature*, *436*, 377–380.

Liu, L.-G. (1975), Post-oxide phases of olivine and pyroxene and mineralogy of the mantle, *Nature*, *258*, 510–512.

Mao, W. L., et al. (2005), Iron-rich silicates in the Earth's D″ layer, *Proc. Natl. Acad. Sci. U. S. A.*, *102*, 9751–9753.

McCammon, C. (1997), Perovskite as a possible sink for ferric iron in the lower mantle, *Nature*, *387*, 694–696.

Monkhorst, H. J., and J. D. Pack (1976), Special points for brillouin-zone integrations, *Phys. Rev. B*, *13*, 5188–5192.

Murakami, M., K. Hirose, N. Sata, and Y. Ohishi (2005), Post-perovskite phase transition and mineral chemistry in the pyrolitic lowermost mantle, *Geophys. Res. Lett.*, *32*, L03304, doi:10.1029/2004GL021956.

Musgrave, M. J. P. (1970), *Crystal Acoustics*, Holden-Day, Boca Raton, Fla.

Ono, S., and A. R. Oganov (2005), In situ observations of phase transition between perovskite and CaIrO₃-type phase in MgSiO₃ and pyrolitic mantle composition, *Earth Planet. Sci. Lett.*, *236*, 914–932.

Perdew, J. P., J. A. Chevary, S. H. Vosko, K. A. Jackson, M. R. Pederson, D. J. Singh, and C. Fiolhais (1992), Atoms, molecules, solids, and surfaces—Applications of the generalized gradient approximation for exchange and correlation, *Phys. Rev. B*, *46*, 6671–6687.

Rost, S., E. J. Garnero, Q. Williams, and M. Manga (2005), Seismological constraints on a possible plume root at the core-mantle boundary, *Nature*, *435*, 666–669.

Stackhouse, S., J. P. Brodholt, J. Wookey, J.-M. Kendall, and G. D. Price (2005), The effect of temperature on the seismic anisotropy of the perovskite and post-perovskite polymorphs of MgSiO₃, *Earth Planet. Sci. Lett.*, *230*, 1–10.

Stackhouse, S., J. P. Brodholt, and G. D. Price (2006), Elastic anisotropy of FeSiO₃ end-members of the perovskite and post-perovskite phases, *Geophys. Res. Lett.*, *33*, L01304, doi:10.1029/2005GL023887.

Wang, Y., and J. P. Perdew (1991), Correlation hole of the spin-polarized electron-gas, with exact small-wave-vector and high density scaling, *Phys. Rev. B*, *44*, 13,298–13,307.

Wookey, J., S. Stackhouse, J.-M. Kendall, J. P. Brodholt, and G. D. Price (2005), Efficacy of post-perovskite as an explanation for lowermost-mantle seismic properties, *Nature*, *438*, 1003–1007.

————————————

J. P. Brodholt, D. P. Dobson, G. D. Price, and S. Stackhouse, Department of Earth Sciences, University College London, Gower Street, London WC1E 6BT, UK. (s.stackhouse@ucl.ac.uk)